

Ductility of open piled wharves under reversed cyclic loads

Hiroshi Yokota[†]

Port and Airport Research Institute, Yokosuka, Japan

Hazem M.F. El-Bakry[‡]

Structural Engineering Department, Alexandria University, Alexandria, Egypt

Abstract. Ductility of open piled wharves under reversed cyclic loads has been investigated. Experimental testing of five wharf models having a scale of about 1:4 was conducted under the application of horizontal reversed cyclic loading. The experiments were designed to focus on the horizontal ultimate load, ductility and failure mode of the considered wharf models. Nonlinear numerical analyses using the finite element method were also performed on numerical models representing the experimentally tested wharves. The results of the experimental tests showed that open piled wharves possessed favourable ductile behaviour and that their load bearing capacity did not depreciate until a ductility factor of 3 to 4 was reached. The numerical analysis showed that the relative rotation that took place at the joints between the steel piles and the R.C. beam was responsible for a considerable portion of the total horizontal deformation of the wharves. Therefore, it was concluded that introducing the joint stiffness in calculating the deformations of open piled wharves was important to achieve reasonable accuracy.

Key words: open piled wharf; steel pile; seismic design; ultimate stage; experimental tests; nonlinear analysis.

1. Introduction

Open piled wharves are widely used in Japanese ports as piers and berthing structures. A typical open piled wharf consists of a reinforced concrete (R.C.) or prestressed concrete (P.C.) platform resting on steel pipe piles. Existing open piled wharves were so designed that they remain elastic and the stresses in their structural members do not exceed allowable limits under the effect of the worst loading conditions including seismic forces (Ministry of Transport 1991). However, the overall structure does not suddenly collapse once the stresses at any structure member exceed the allowable values as a result of being subjected to seismic loads higher than the design predicted ones. This reserve of strength is justified by the high degree of indeterminacy and the failure mode of the wharves which reach their ultimate load after experiencing several local failure events such as yielding and plastic hinge formation in steel piles and yielding of rebars in the R.C. deck. Therefore, seismic performance of open piled wharves can be expected to be higher than the design

[†] Head of Division
[‡] Lecturer

assumptions and this has been already confirmed by the results of site observations and numerical analyses (Yokota *et al.* 1998a and 1998b).

After studying the damage that took place in many Kobe port structures during the 1995 Hyogoken-Nambu earthquake, it was concluded that Level 2 earthquakes which have a return period of several hundred years should be accounted for when designing port structures. Research is currently under way to establish new design methods which allow structures to undergo controlled inelastic deformations without collapsing in the event of a major earthquake (Werner 1998). To achieve such design criteria, it is important to fully understand the behaviour of open piled wharves up to the ultimate stage and be able to assess the reserve of load-carrying capacity and ductility which these structures have beyond their elastic limit.

To investigate the structural performance of open piled wharves under seismic loads, a series of experimental tests have been conducted on five $\approx 1:4$ scale wharf models. Also, nonlinear numerical analysis was carried out using the finite element method to simulate the behaviour of the studied models. In this paper, the results of the experimental tests were discussed in terms of the mode of failure, ultimate load and displacement ductility. The displacement ductility mentioned in this paper is defined as the ratio between the maximum horizontal deformation of the models at the ultimate load and that at the first yielding of the piles. Also, a comparison was made between the results obtained from the experimental testing and those obtained from the numerical analysis.

2. Experimental testing

Five open piled wharf models, having a scale of about 1:4 to average prototypes, were manufactured and loaded using reversed cyclic lateral loading up to failure. Each model represented one row of piles with its corresponding part of R.C. deck. The objectives of this test programme were to study the displacement ductility and the mode of failure of the wharf models. Furthermore, close attention was paid to the relative movements which took place at the joints between the steel piles and the R.C. deck.

In an actual open piled wharf, most of the pile part is submerged in water which might affect its dynamic response during an earthquake. However, during the seismic design stage of an open piled wharf, the existence of water should be accounted for in determining the characteristics of the dynamic behaviour such as response acceleration, displacements and seismic forces. The structural calculations are then carried out using static forces which are equivalent to the calculated seismic ones. Therefore, the loading tests considered in this work were conducted under reversed cyclic forces in the air and were assumed sufficient to achieve the stated objectives.

2.1 Test models

Fig. 1 shows the geometrical shape and dimensions of the five tested wharf models. Each of the specimens consisted of steel pipe piles fixed to a R.C. beam at the top and a R.C. base at the bottom. Two of the specimens (W1 and W2) had a two-pile configuration and the remaining three (W3, W4 and W5) had a three-pile configuration. As the piles of an actual open piled wharf are driven into the ground, it is necessary to reproduce the ground-structure interaction when studying specimens in the laboratory. It is common in usual design procedures to assume virtual fixed points at the piles a few metres below the ground surface and to analyse the structure above these points

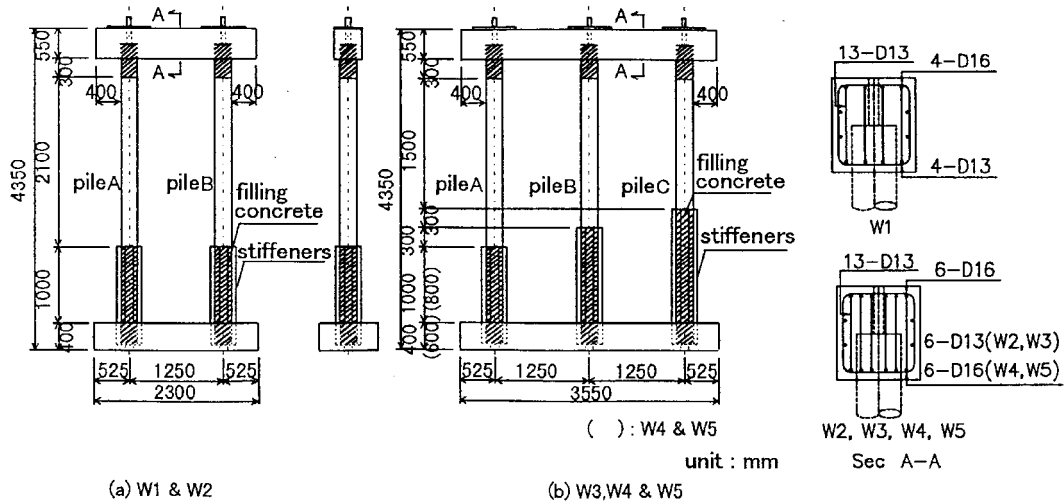


Fig. 1 Geometry and dimensions of test models

as a rigid frame. This assumption of the existence of virtual fixed points was adopted for the experimental test models. For this purpose, steel stiffeners were welded to the sides of the steel piles in their lower portions, which were also filled with concrete, to represent the confined parts of the piles below the virtual fixed points. Models W1 and W2 represented cases where the ground surface was horizontal and models W3, W4 and W5 represented cases of inclined ground surface.

Steel pipes of 267 mm in diameter \times 5.8 mm in thickness, which were thicker than average prototypes, were used for the piles of W1, W2 and W3 while pipes of 267 mm \times 4 mm, which had almost the same proportions as average prototypes, were used for the piles of W4 and W5. The top R.C. beam had cross section dimensions of 500 mm in width and 550 mm in height for all the models. The longitudinal reinforcements varied for the different models and are shown in Fig. 1. The arrangement of W3's beam reinforcement, as an example, and the details of the bottom rebar near the piles are shown in Fig. 2. While the top rebar were continuous over the piles, the bottom rebar were cut and welded to the piles using splice plates. The R.C. base at the bottom of the piles

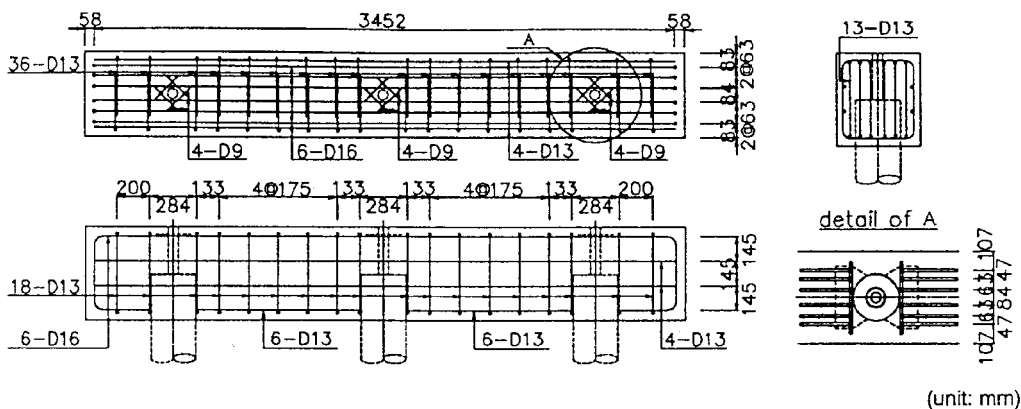


Fig. 2 Details of R.C. beam reinforcements (W3)

had a cross section 800 mm wide and 400 mm high for models W1, W2 and W3 and 800 mm wide and 600 mm high for models W4 and W5.

The concrete used for the R.C. beam/base and the filling of piles had a normal mix with a maximum size of coarse aggregate of 20 mm. Concrete core specimens of 100 mm in diameter were cut out from sound uncracked parts of the R.C. base after the loading tests. Compression tests were performed on the core specimens and the average compressive strength of the concrete was 37 N/mm². The R.C. beams/bases were reinforced using deformed steel bars having yield stress of 371 N/mm² and tensile strength of 501 N/mm². The yield stress and tensile strength for the steel piles were 369 N/mm² and 462 N/mm² respectively.

2.2 Test setup and instrumentation

The experimental models were tested in a horizontal alignment, as shown in Fig. 3 for W1/W2 as an example. The base of each model was fixed to a reaction wall using high strength bars. According to the seismic design of the wharves, it is assumed that principal seismic forces would act on the R.C. deck at its centre of gravity. Therefore, a double action (pushing/pulling) hydraulic jack was placed to apply lateral static force along the centreline of the R.C. beam. Axial forces were introduced at the centreline of each pile to account for the gravitational loads due to the self weight and surcharge on the deck. These axial forces were applied by prestressing wires, placed inside each pile, using hydraulic jacks as shown in Fig. 3.

The adopted instrumentation of W3, as an example, is shown in Fig. 4. To avoid complexity in the drawing, the positions of strain gauges are shown only for pile A and those of displacement transducers are shown only for pile C. Similar positions for both kinds of measurements were adopted for all piles. Fig. 5 shows the special displacement transducers placed at the corners between the piles and the R.C. beam/base to monitor the relative rotations which took place at these

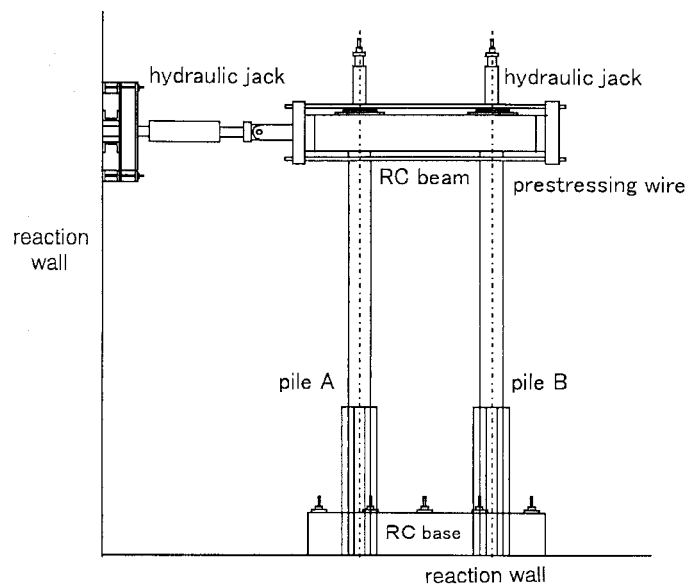


Fig. 3 Test setup

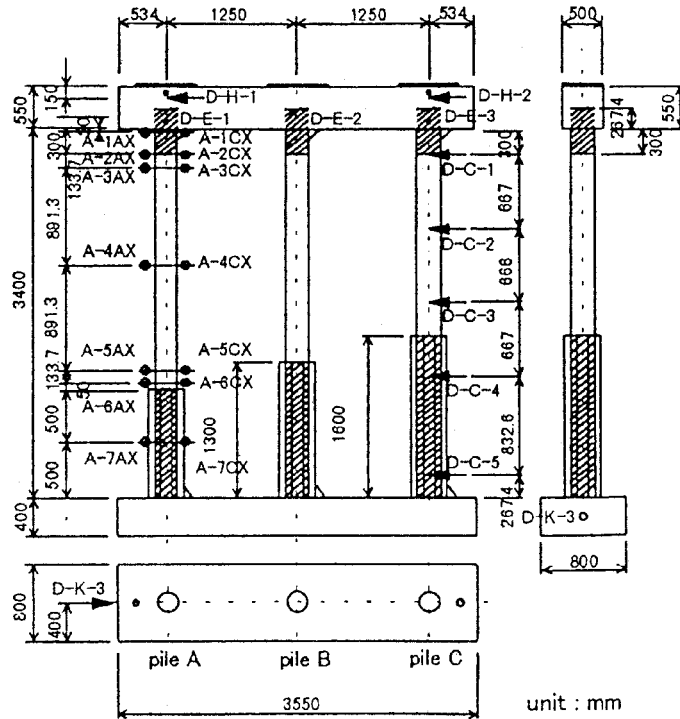


Fig. 4 Instrumentation of W3

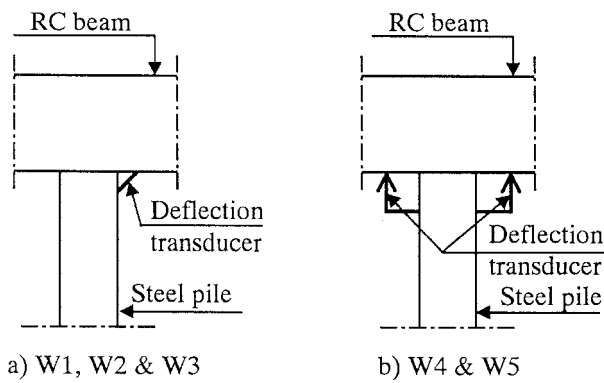


Fig. 5 Displacement transducers at the joints

joints. These measurements were later transformed into rotation angles.

2.3 Test procedures

Each test was conducted by, first, prestressing the wires inside the steel piles to produce axial

forces of 200 kN at each pile. These forces were equivalent to the weight of the wharf and a uniform surcharge of 10 kN/m² during an earthquake. These prestressing forces were not adjusted, after their initial application, throughout the course of each test for models W1, W2, W3 and W4. However, for W5, the prestressing force was monitored and re-adjusted to its initial level after the application of each horizontal load increment during the test.

After the prestressing process was complete, a reversed cyclic lateral load, which corresponded to the seismic force, was applied at the level of the R.C. beam using the hydraulic jack. The lateral load was applied according to displacement controlled alternating cycles. The first loading cycle was performed by gradually applying the lateral load in the pushing (+ve) direction until the extremely stressed steel pile fibres reached yielding. The corresponding maximum lateral displacement δ_y , at the R.C. beam level, was then recorded and the lateral load was then completely released. The same procedure was repeated in loading in the pulling (-ve) direction. This cycle of pushing-releasing-pulling-releasing was performed three times for each of the displacement values of δ_y , $2\delta_y$, $3\delta_y$ and $4\delta_y$. For loading cycles reaching displacement values beyond $4\delta_y$, the number of cycles was determined according to the progress of each test. The loading cycles continued with escalating values of the maximum lateral displacement till the complete collapse of each model.

At each loading step, a complete set of measurements of the applied loads, strain values and displacements was recorded. Also, crack propagation on the surfaces of the R.C. beam and local buckling of the steel piles were visually observed and marked during the tests.

3. Numerical modelling

Five numerical models, representing the respective five experimentally tested wharf models, were studied using nonlinear finite element analysis. The analysis was carried out to investigate the feasibility of predicting the behaviour of open piled wharves using a numerical technique. In practical design procedures, rigid connections between the steel piles and the R.C. deck are assumed. To study the effect of the joint performance on the overall behaviour of the wharves, two cases for the stiffness of the joints between the steel piles and the RC beam/base were considered in the numerical analysis. The first case was a rigid connection between the piles and the RC beam/base and the second case was a flexible connection with flexural stiffness as obtained from the experimental results. The details of the geometry and material models adopted in the numerical analysis are as follows:

3.1 Geometry

Fig. 6 shows the geometry of the numerical model used for the finite element analysis of the three-pile configuration wharf models (W3, W4 and W5). Similar modelling for the steel piles and the R.C. beam was adopted for the two-pile configuration wharf models (W1 and W2). The R.C. beams were modelled using 4 and 8 beam elements for the two-pile models and the three-pile models respectively. All longitudinal rebars were considered in the cross section of the beam elements. The steel piles were also modelled using beam elements and were divided into three parts according to the presence of concrete filling and stiffeners. The corresponding cross section properties were used for each part and equivalent steel sections were used where concrete filling was present.

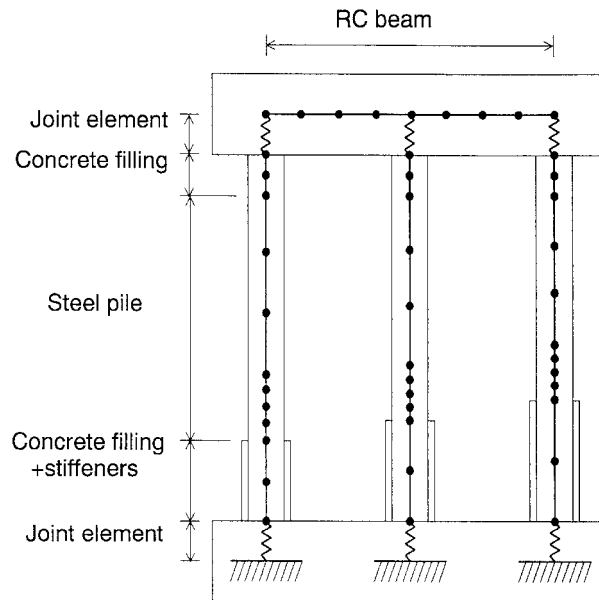


Fig. 6 Geometry of the numerical models

To study the effect of the joint stiffness on the overall behaviour of the wharves, additional beam elements were introduced to represent the parts of piles embedded in the beams. The properties of these beam elements were defined by their moment-curvature relationship to account for the relative rotation that took place at the joints between the piles and the R.C. beam. During conventional design to existing wharves, the joint stiffness was not so important because this was considered to be rigid enough under the allowable stress level. In the new design method, however, the rotational movements there may not be ignorable because the structural behaviour with large displacement is to be taken into account. This is why the flexible beam elements were introduced in this numerical model.

3.2 Materials

The material properties used for the finite element analysis were obtained from tensile and compressive tests on steel and concrete specimens respectively. Tensile specimens for steel rebars and piles were taken from representative samples and compressive specimens for concrete material were core cylinders cut out from sound concrete parts of the R.C. base after the testing of the wharves.

The properties of the beam elements representing the parts of the piles embedded in the R.C. beam/base were determined from the experimental measurements recorded during the testing of the wharves. The measurements obtained from the displacement transducers, at the corners of the joints between the piles and the beams/bases (Fig. 5) were used to calculate the relative angles of rotation at these joints. These angles of rotation were transformed to curvature values assuming that the rotation took place over a length of the piles equal to 275 mm which was half the height of the R.C. beam. This was the same length of the parts of the piles embedded in the R.C. beam as considered in the numerical models. The corresponding bending moments at the joints were

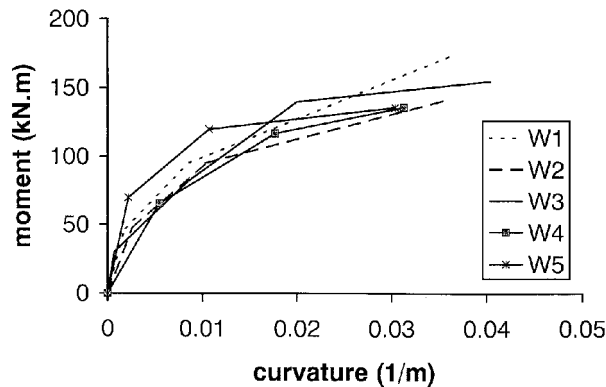


Fig. 7 Stiffness of top joints

calculated from the measured piles axial strains. Strain values at stations 4 and 7 (as shown in Fig. 4) of each pile, as they were below yield values throughout the tests, were used to calculate the bending moments at these stations. The bending moments at the top and bottom joints were then calculated by linear extrapolation using the moments at sections 4 and 7 of each pile. Samples of the moment-curvature relations obtained using the aforementioned procedure are shown in Fig. 7 for the top joints of the five tested wharf models. A different set of relations was obtained for the bottom joints of each model. The difference between the behaviour of the top joints and that of the bottom joints was attributed to the different dimensions and reinforcement of the top beam and the bottom base and the existence of the stiffeners at the bottom end of the piles. These experimentally obtained moment-curvature relations were assigned to the beam elements representing the parts of the piles embedded in the R.C. beams/bases.

4. Results and discussions

4.1 Progress of failure

In the first test, W1, cracking of concrete started to appear at the bottom surface of the R.C. beam near pile A at a pushing load of 118 kN (see Fig. 4 for the positions of the different piles and sections). Afterwards, cracks appeared on the top surface of the beam near pile B and the side surface near pile A. During the application of pulling loads, cracks occurred at the top surface of the R.C. beam near pile A and the side surface near pile B. At a lateral displacement of $-2\delta_y$, a diagonal crack was observed at the side surface of the beam. Fig. 8 shows the crack pattern of the top, side and bottom surfaces of the R.C. beam. Local buckling of the steel piles took place at sections A-6 and B-6 at lateral displacement values of $3\delta_y$ and $-3\delta_y$, respectively. After the occurrence of local buckling, the lateral load did not increase as the lateral displacement was increased up to $6\delta_y$. At a lateral displacement of $4\delta_y$, a crack at the top surface of the beam near pile A propagated and reached the opposite surface. Since the ultimate load was confirmed at $4\delta_y$, one loading cycle was performed for each controlling displacement value afterwards. As the lateral displacement was increased, the cracks became wider and significant cracks appeared along the longitudinal rebars at the bottom surface of the beam at $6\delta_y$. The concrete cover at the bottom

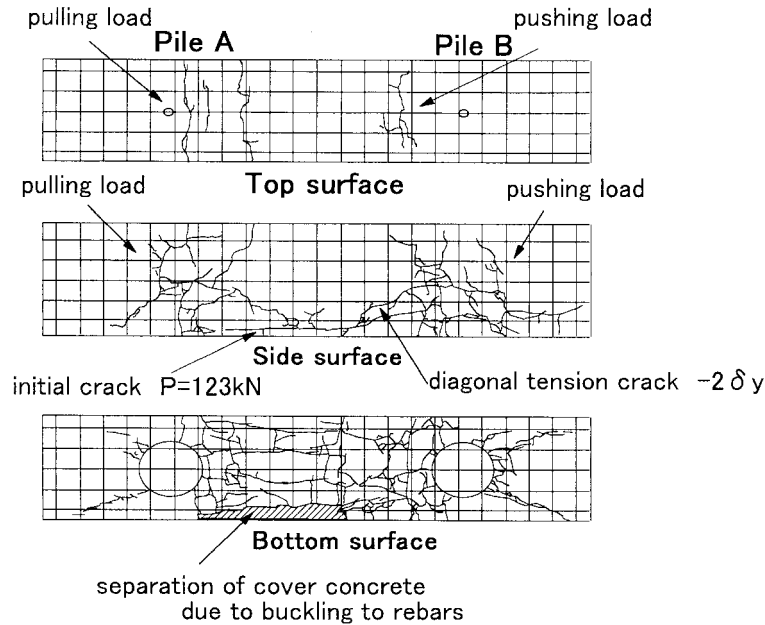


Fig. 8 Crack pattern of R.C. beam of W1

surface of the beam fell off as the longitudinal rebars buckled between the two piles. Local buckling of the steel piles at sections A-2 and B-2 was then confirmed. The test was then terminated as the lateral load notably decreased at $-6\delta_y$. A summary of the sequence of local failure events is shown in Fig. 9.

Model W2, with a higher reinforcement ratio for the R.C. beam, showed almost the same pattern of cracks. The first crack appeared at a lateral load level of 123 kN, a value slightly higher than that of W1 which could be attributed to the higher reinforcement ratio of W2 compared to W1. The sequence of local failures up to $6\delta_y$ followed a behaviour similar to that described earlier for W1.

During testing of W3, cracks were initially observed on the side surface of the R.C. beam near pile A and on the top surface near pile C at a lateral load level of 157 kN. As the lateral displacement was increased, cracks further developed near pile A and pile C with only a few cracks in the vicinity of pile B. Local buckling of steel piles was observed at sections B-2, B-6 and C-6 at a lateral displacement of $4\delta_y$. While local buckling of pile B started at its top section and then occurred at the bottom, the local buckling of pile C started at the bottom and then occurred at the top. This could be attributed to the moment concentration at the top of pile B attracted by the stiff, relatively uncracked, portion of the R.C. beam near the top of this pile. On the other hand, the developed cracks near the top of pile C resulted in a partial release of the bending moment at this end and shifted the critically stressed section to the bottom of the pile. At $5\delta_y$, considerable cracking occurred and, eventually, the concrete cover at the bottom surface of the beam between pile B and pile C fell off at $6\delta_y$. Fig. 10 shows a summary of the sequence of local failure events of W3.

During the testing of W4, no cracks were observed at a displacement value of δ_y which was different from the case of W3 where cracks have already developed at this displacement value. This could be attributed to the lower bending moments at the beam sections due to using piles with thinner walls for W4 (pile thicknesses were 5.8 mm and 4 mm for W3 and W4 respectively).

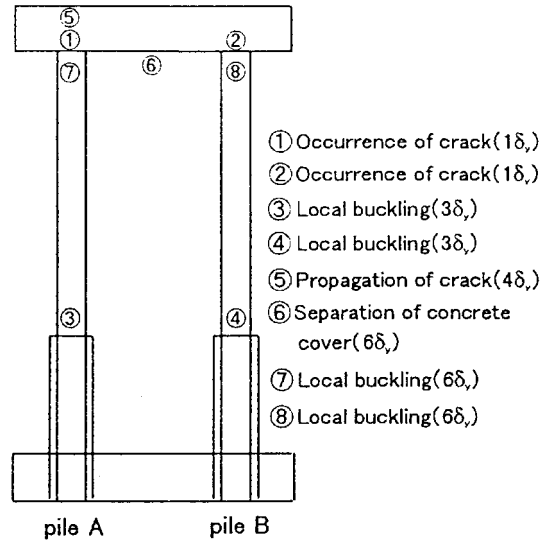


Fig. 9 Progress of local failures of W1

Concrete cracking was initiated near pile A at $2\delta_y$, which corresponded to a lateral load level of 216 kN. When the load was applied in the $-ve$ direction, concrete cracking was initiated near pile C at $-2\delta_y$ corresponding to a load level of -196 kN. The local buckling of piles was first observed at section C-6 at $3\delta_y$. As the lateral displacement was increased in subsequent cycles, local buckling occurred at sections B-6 and A-6 then at sections B-2 and C-2 at $4\delta_y$. At $-5\delta_y$, local buckling occurred at section A-2. A summary of the sequence of the local failure events is shown in Fig. 11.

Model W5 had its pile axial loads monitored and re-adjusted to their initial values after every

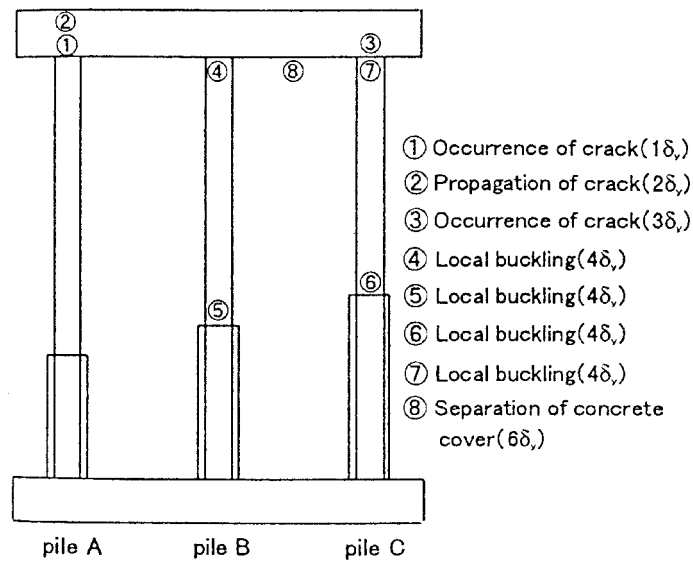


Fig. 10 Progress of local failures of W3

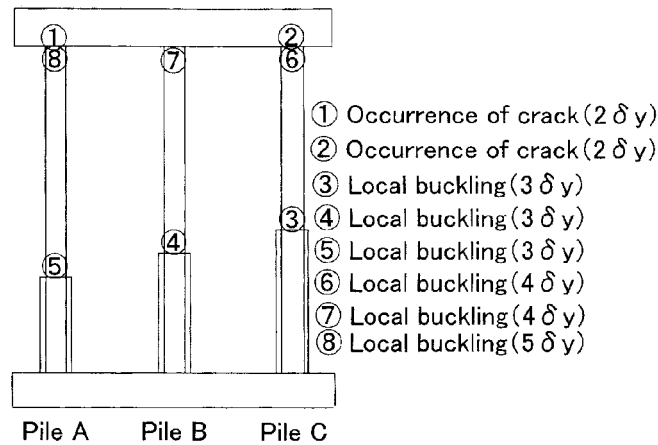


Fig. 11 Progress of local failures of W4

lateral load increment. The propagation of cracks started at $2\delta_y$ near pile A at a lateral load of 206 kN. In the $-ve$ direction, the first crack was observed at $-2\delta_y$ near pile C at a lateral load of -196 kN. Local buckling occurred at sections B-6, A-6 and C-6 at $3\delta_y$ followed by local buckling at section C-2 at $4\delta_y$, and A-2 and B-2 at $-4\delta_y$.

The axial forces applied by prestressing on the piles were found to remain almost unchanged during the course of all tests until the ultimate load was reached. As the lateral pushing/pulling continued past the peak load with the development of local buckling of the piles, the axial load depreciated. This was attributed to the partial loss of prestress due to the high axial deformations of the piles caused by local buckling of their critical sections.

4.2 Horizontal deformations

Fig. 12 shows the relationship between the lateral displacements and the corresponding lateral loads for W1. The first recorded yielding during the loading of W1 in the $+ve$ direction was at section B-2 and the corresponding basic lateral displacement, δ_y , was 27.15 mm at a lateral load of 132 kN. When the load was applied in the $-ve$ direction, the first yield occurred at section A-2 at a lateral load level of 137 kN. In the following two cycles of loading up to the same controlling displacement value of $\pm \delta_y$, the load-displacement path followed the same curve and the maximum load of each cycle did not depreciate. The ultimate load was reached in the first cycle of loading up to $3\delta_y$, and depreciated in subsequent cycles reaching about 80% of its ultimate value at $6\delta_y$. The depreciation of the applied load coincided with the occurrence of the local buckling at the most stressed sections of the piles. The lateral load-displacement relationship of W2 was similar to that of W1, as can be seen in Fig. 13, although the reinforcement ratios of their top beams were different.

The first yield of W3 took place at section C-1 at a lateral displacement, δ_y , of 25.40 mm and a corresponding load level of 220 kN (Fig. 14). As the applied lateral displacement was increased, the corresponding load increased until the first cycle of the displacement value of $4\delta_y$ was reached. After that, the lateral load depreciated in subsequent cycles until it reached about 80% of its ultimate value at a displacement value of $6\delta_y$. As the applied load did not depreciate before a displacement value of $4\delta_y$ was reached, it could be stated that a displacement ductility factor of 4

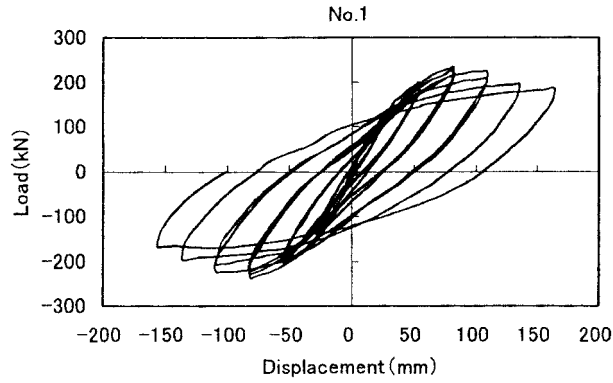


Fig. 12 Experimental lateral deformations of W1

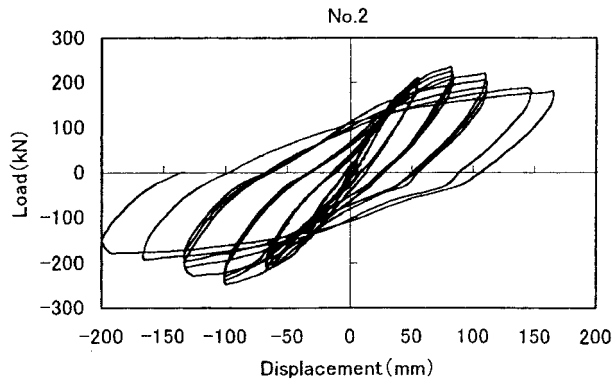


Fig. 13 Experimental lateral deformations of W2

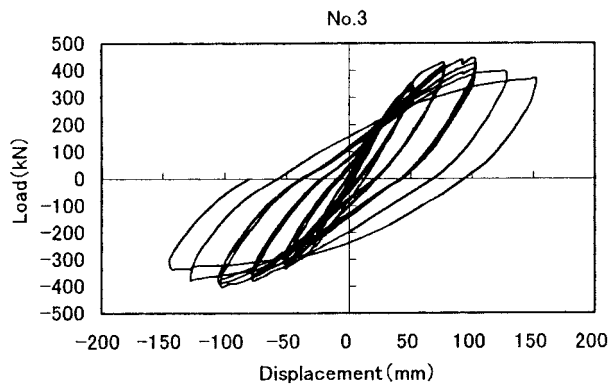


Fig. 14 Experimental lateral deformations of W3

was satisfied. The same value was proposed by Kimura *et al.* (1998) as the allowable displacement ductility for footings on prestressed concrete pile foundations.

The load-displacement relationship for W4 is shown in Fig. 15. The first yield was recorded at section C-6 at a lateral displacement, δ_y , equal to 16.20 mm corresponding to a load level of 137

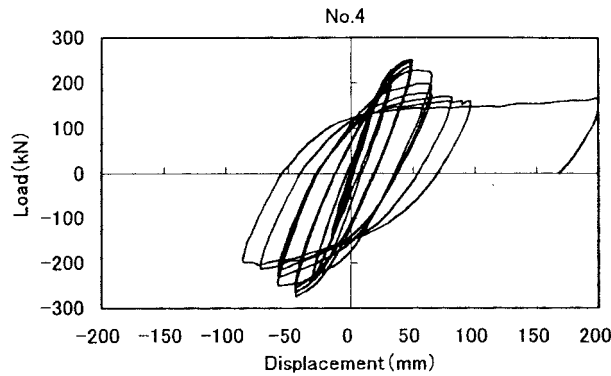


Fig. 15 Experimental lateral deformations of W4

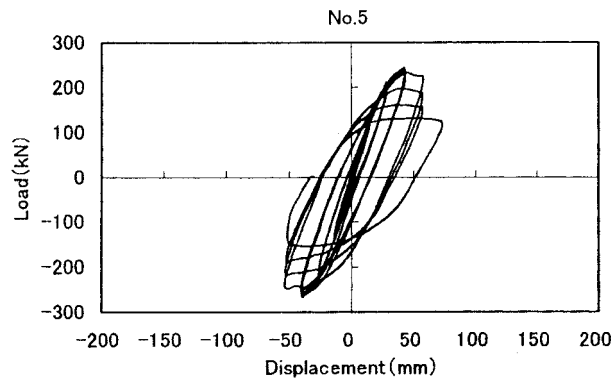


Fig. 16 Experimental lateral deformations of W5

kN. When load was applied in the $-ve$ direction, the first yield took place at section B-2 at a load level of -147 kN and a corresponding displacement of -14.60 mm. The ultimate load was recorded at the first cycle of $3\delta_y$ and started to decrease in the following two cycles of $3\delta_y$. At $4\delta_y$, the maximum cycle load considerably depreciated and reached about 60% of its ultimate value at $6\delta_y$. A generally similar performance was recorded for W5 as can be seen in Fig. 16. The value of δ_y for W5 was 14.40 mm corresponding to the occurrence of first yield at section B-6 at a load level of 127 kN. Under $-ve$ loading, the first yield was recorded at section A-6 at a lateral displacement of -13.40 mm and a corresponding load of -137 kN.

Reviewing the behaviour of the tested models revealed that the degradation of their lateral stiffness started at the occurrence of the first yield of each model. This suggested that the occurrence of the first yielding event could be considered as the elastic limit of the wharves. However, previous analytical results by Yokota *et al.* (1998b) showed that the elastic limit was defined by the formation of plastic hinges, not the first yield. This difference could be justified by the actual soil-pile interaction that was not properly modelled in the test specimens. It was believed that the fixation of the models bases to the reaction wall and the stiffeners added to the piles at their lower parts overestimated the restraining effect of the soil on the piles. This led to the occurrence of the first yielding and the formation of the plastic hinges, at the lower sections of the piles, at load

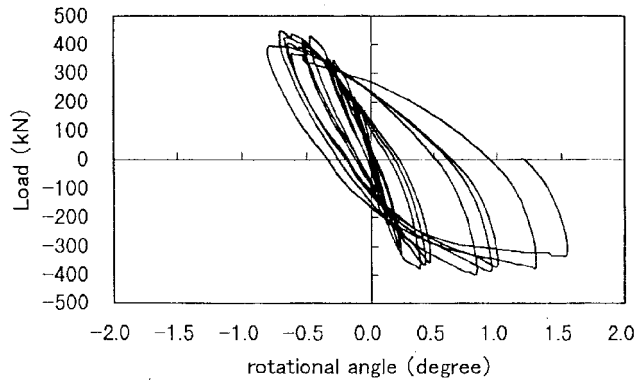


Fig. 17 Experimental relative rotation at the top of pile B of W3

levels lower than what would be expected if the piles were actually driven into the ground and surrounded by soil.

4.3 Relative rotation of the joints

Relative rotations between the ends of steel piles and the surrounding concrete were observed in all the experiments. These rotations were noted starting from the early stages of loading and showed more clearly at the ultimate stages. Fig. 17 shows an example of the measured relative rotation at the top of pile B of W3. As can be seen in the figure, the angle of rotation reached about 1 to 1.5 degrees at the ultimate load of the model. At this stage, it was believed that this relative rotation could have a considerable contribution to the overall deformations of the wharf models.

4.4 Analytical results

The relationships between the lateral displacements and the applied loads obtained from the finite element analysis for both cases of rigid and flexible joint assumptions are shown in Figs. 18 to 22 for all the studied wharves. The figures also show comparisons with the experimental results. The envelopes of experimental load-displacement relationship are drawn in these figures. From these graphs, it can be seen that the analytical results, when using the flexible joint assumption, were in good agreement with the experimental ones as far as both the lateral displacements and the ultimate loads were concerned. However, for W4 and W5, with relatively thin pile walls, the lateral displacements near the ultimate loads were slightly underestimated. This could be attributed to the deformations resulting from the local buckling of the piles that showed more clearly in these two models which were perhaps not properly modelled in the numerical analysis.

Ignoring the actual stiffness of the joints and assuming rigid connections between the steel piles and the R.C. beam/base resulted in a significant underestimation of the lateral deformations of the studied wharf models. At the first occurrence of pile yielding, the lateral displacements depicted using the rigid joint assumption were only 55% to 77%, with an average value of 64%, of the displacements obtained using the flexible joint assumption. At the ultimate load, the lateral displacements depicted using the rigid joint assumption were only 35% to 72%, with an average value of 54%, of the displacements obtained using the flexible joint assumption although the

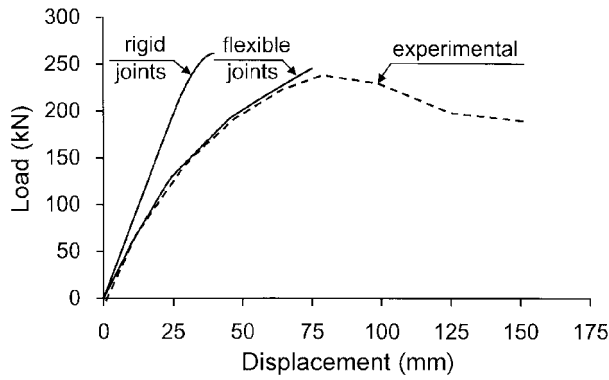


Fig. 18 Analytical lateral deformations of W1

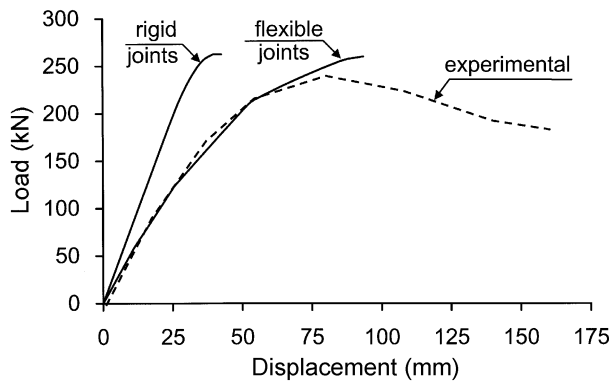


Fig. 19 Analytical lateral deformations of W2

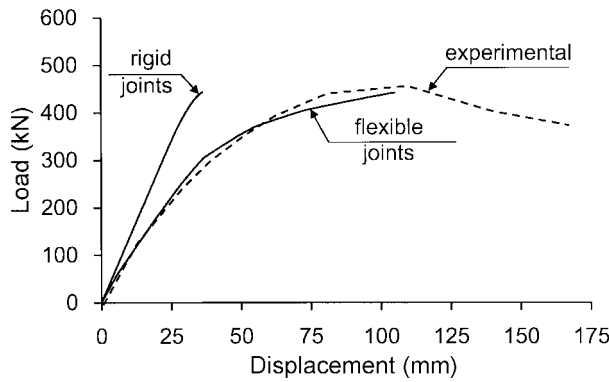


Fig. 20 Analytical lateral deformations of W3

ultimate loads were almost the same. The deviation between the two analytical curves increased as the loads approached their ultimate limits where the joints stiffness notably deteriorated. This indicated that the relative rotations that took place between the piles and the beams/bases were major contributors to the overall displacements of the wharves and that it is important to introduce

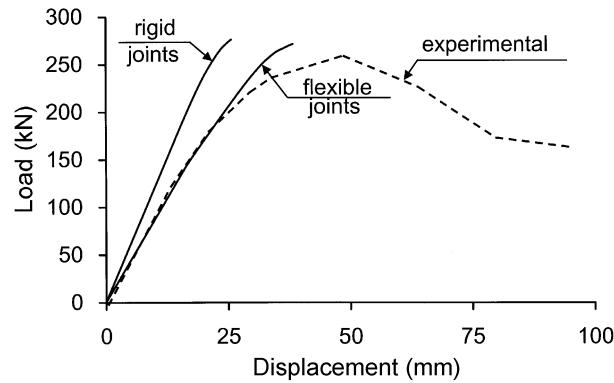


Fig. 21 Analytical lateral deformations of W4

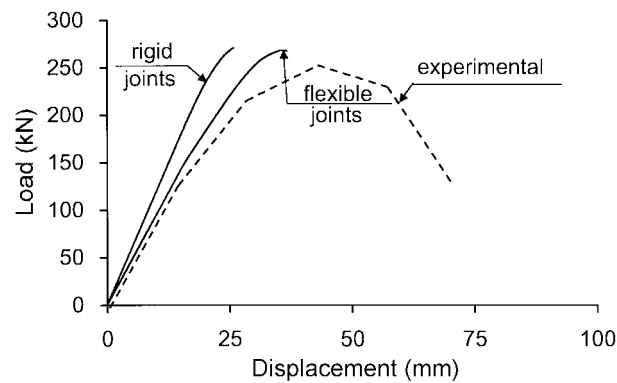


Fig. 22 Analytical lateral deformations of W5

joint stiffness in the analysis of open piled wharves if the lateral displacements are sought.

The sequence of damage events, concrete cracking and yielding of pile sections, depicted by the analytical results, according to the flexible joint assumption, almost coincided with the experimental observations. Yielding of piles and plastic hinges formation started generally at the bottom of the piles and then spread to the top in all the studied models. However, when rigid joints were assumed, yielding of pile sections and plastic hinge formation were depicted at the top of the piles at first and then spread to the bottom ends. This indicates the effect of the joints stiffness on the progress of failure of open piled wharves. Fig. 23 shows an example of the sequence of damage events that took place in W3 according to the analytical results in both cases of flexible and rigid joint assumptions. The yielding events shown in the figure depict the pile locations, A, B and C, the end of the pile, top and bot (bottom), and the type of yield, C (compression) and T (tension). This graph shows that all yielding events that took place at the top of the piles when assuming rigid joints were earlier than the corresponding events that took place when assuming flexible joints. Similarly, all yielding events that took place at the bottom of the piles when assuming rigid joints were later than the corresponding events that took place when assuming flexible joints. The same argument could be applied to all the considered models. This could be attributed to the partial release of bending moment at the top joints, due to their higher flexibility compared with the bottom ones, on the

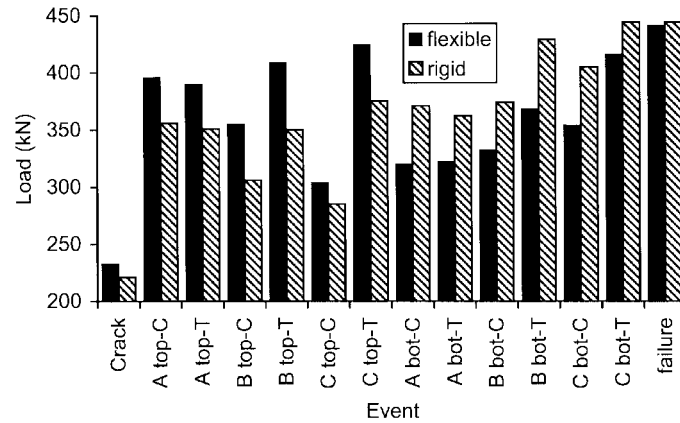


Fig. 23 Sequence of damage events of W3

account of the increase in the bending moments at the bottom ends of the piles. This further illustrates the importance of introducing the actual joint stiffness in the analysis of open piled wharves. If rigid joints are assumed in the analysis, a false pattern for the progress of failure could be obtained.

5. Conclusions

From the experimental and analytical work presented in this paper, the following conclusions have been drawn:

- (1) The horizontal load carrying capacity of the studied open piled wharves did not depreciate before a horizontal displacement of about 3 to 4 times the displacement at the first yield of the piles was reached. Therefore, the displacement ductility ratio of 3 to 4, required for design for earthquakes, was satisfied.
- (2) The normally adopted assumption of a rigid connection between the steel piles and the R.C. deck is not adequate for predicting the horizontal displacement and the sequence of the progress of failure under seismic loads.
- (3) Introducing the effect of joint stiffness in the finite element analysis resulted in a good prediction of the experimental behaviour of the tested wharf models.
- (4) The rigid joint assumption underestimated the horizontal displacements of the studied wharf models by 36% and 46%, on average, compared with the flexible joint assumption at the first yield loads and the ultimate loads, respectively.

Acknowledgements

The authors would like to thank Messrs N. Kawabata, S. Kawasaki and R. Sugawara for their assistance in preparing and conducting the experimental tests.

References

- Kimura, Y., Okoshi, M., Nakano, M., Fukui, J., and Yokoyama, K. (1998), "An experimental study on the ductility of pile foundations", *J. Struct. Eng.*, JSCE, 44A, 1597-1606.
- Ministry of Transport (1991), "Technical standards for port and harbour facilities in Japan", The Overseas Coastal Development Institute of Japan, 286-295.
- Werner, S. D.(1998), "Seismic guide lines for ports", ASCE, 6.13-6.49.
- Yokota, H., Takehana, N., Minami, K., and Kawabata, N. (1998a), "Consideration on the earthquake resistant design of an open type wharf with steel piles", *J. Struct. Eng.*, JSCE, 44A, 1613-1622.
- Yokota, H., Kawasaki, S., Sugawara, R., and Kawabata, N. (1998b), "Parametric study on ductility design of open wharves supported on vertical pile system", *Proc. 2nd Symp. on Ductility Design Method for Bridges*, JSCE, Tokyo.